http://dx.doi.org/10.11142/jicems.2013.2.2.159
Journal of International Conference on Electrical Machines and Systems Vol. 2, No. 2, pp. 159~164 , 2013

Improved Torque Calculation of High Speed Permanent Magnet Motor with Compressor Loads Using Measured Power Factor Angle and Analytical Circuit Parameters

Jang-Young Choi*, Seok-Myeong Jang* and Sung-Ho Lee**

Abstract – Difficulty of torque measurements in high-speed permanent magnet (HSPM) motors has necessitated the development of improved torque calculations. Hence, this paper presents an analytical torque calculation of a high speed permanent magnet (HSPM) motor based on the power factor angle. On the basis of analytical magnetic field solutions, the equations for circuit parameters such as back-emf and synchronous inductance are derived analytically. All analytical results are validated extensively by non-linear finite element (FE) calculations and measurements. The internal angle (δ) between the back-emf and the phase current is calculated according to the rotor speed by using analytical circuit parameters and the measured power factor because this angle is not measured but estimated in case of sensorless drive of the HSPM motor, significantly affecting torque calculation. Finally, the validity of the torque analysis method proposed in this paper is confirmed, by showing that the torque calculated on the basis of the internal angle is in better agreement with the measurements.

Keywords: High-speed permanent magnet motors, analytical torque calculations, FE calculations, power factor

1. Introduction

High speed permanent magnet (HSPM) machines are likely to be a key technology for many future applications of air-compressor systems, owing to their high efficiency, small size, and light weight [1-2]. In order to measure efficiency of air-compressor systems with HSPM motors, it is very important to measure torque of HSPM motors. Generally, the torque of electric machines can be easily measured by using a torque sensor or a dynamometer. However, there are many problems associated with measuring the torque of HSPM motors owing to speed limits (exceeds 50,000rpm) and the cost of measuring devices. Moreover, it is impossible to measure torque of HSPM motors with an impeller and a thrust bearing at both sides of their shaft because of absence of space to install torque sensors. Therefore, there has been an increased focus on the accurate prediction of the torque of HSPM motors. There is a strong possibility that a non-zero internal angle (δ) between the back-emf and the input current exists, despite attempts to maintain this angle at δ = 0, because HSPM motors with compressor loads should be operated by sensorless drive and have a large reactance owing to a high operating frequency. Hence, it is very important to consider the internal angle in order to predict the torque of an HSPM motor accurately.

This paper addresses such accurate torque calculation for the HSPM motor by using a power factor angle and analytical circuit parameters. On the basis of the magnetic vector potential and the two-dimensional polar coordinate system, this paper derives analytical solutions for magnetic fields produced by permanent magnets (PMs) and stator winding currents. Analytical solutions for circuit parameters such as a back-emf and a synchronous inductance are also obtained from the derived analytical magnetic field solutions. The analytical results are validated extensively with finite element (FE) analyses and measurements. By using a phasor diagram of the HSPM motor, derived analytical circuit parameters, and power factor angle obtained from test results, the internal angle (δ) is calculated for various rotor speeds. Finally, we confirm that by including the effects of a non-zero δ in our calculations, we obtain a better agreement between the measured and the calculated torque.

* Dept. of Electrical Engineering, Chungnam University, Korea. (choi_jy@cnu.ac.kr)
** Gwangju R&D center of Korea Institute of Industrial Technology
Received 16 May 2013 ; Accepted 24 May 2013

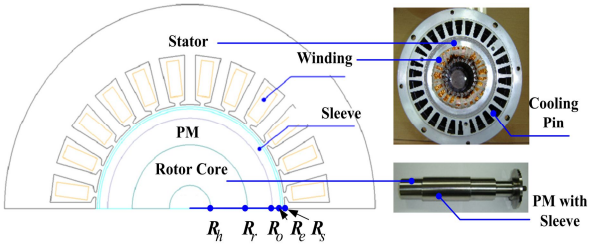

Fig. 1. Schematic and actual model of the HSPM motor with 2-pole rotor and 24-slot stator

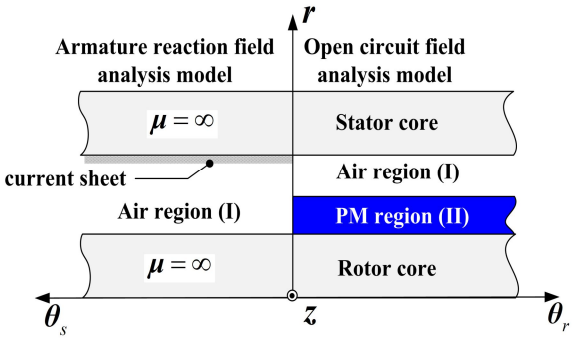

Fig. 2. Simplified analysis model for the prediction of magnetic fields

2. Structures and Analytical Model of HSPM Motor

Figure 1 shows the schematic of the HSPM motor and an image of the actual manufactured model employed in validating the analysis methods presented in this paper. The motor has a 2-pole diametrically magnetized rotor and a 24-slot stator. The geometrical parameters are as follows: inner and outer radii of rotor core, R_h = 5 mm and R_r = 14 mm; inner and outer radii of sleeve, R_o = 20 mm and R_e = 22 mm; inner radius of stator core, R_s = 23 mm; active axial length, l_a = 72 mm; remanent flux density of PMs, B_r = 1.06 T (SmCo); rated power and speed, P_o = 6 kW and N_s = 60,000 rpm.

Figure 2 shows the simplified magnetic field analysis model. In this figure, the relative permeability of the rotor and stator back iron core is assumed to be infinite, while the permeability of the PMs and sleeve is assumed to be unity. The current is also assumed to be distributed in an infinitesimally thin sheet at $r = R_s$. Therefore, as shown in Fig. 2, open-circuit field analysis regions are confined to two regions, namely, the air-gap region (I) and the PM region (II), while the armature reaction field analysis region is confined to only one region, namely, the air-gap region (I). Here θ_r and θ_s are the angle for rotor and stator reference frames, respectively. Their relationship is given by $\theta_r = \theta_s + \omega_r t$. ω_r is the rotor angular speed in (rad/s).

3. Formulation of the Problem

3.1 Magnetic Fields Produced by PMs and Stator Winding Currents

Let us obtain the governing equations for open-circuit field analysis. In the magnet region, $\mathbf{B} = \mu_0(\mathbf{H} + \mathbf{M})$ and $\nabla \times \mathbf{H} = \mathbf{0}$ owing to the absence of free current. Therefore, $\nabla \times \mathbf{B} = \mu_0 \nabla \times \mathbf{M}$. The magnetic vector potential $\mathbf{A}$ is defined as $\nabla \times \mathbf{A} = \mathbf{B}$. Therefore, Laplace's and Poisson's equations in terms of the Coulomb gauge $\nabla \cdot \mathbf{A} = 0$ are given by [3-4]

$$\nabla^2 \mathbf{A}^{\mathbf{I}}{}_{pm} = 0$$
$$\nabla^2 \mathbf{A}^{\mathbf{II}}{}_{pm} = -\mu_0 (\nabla \times \mathbf{M}) \quad (1)$$

where subscript *pm* indicates a magnetic quantity generated by the PMs, μ_0 is the permeability of air, and $\mathbf{M}$ is the magnetization of diametrically magnetized PMs. In a similar manner, the governing equation for armature reaction field analysis is given by

$$\nabla^2 \mathbf{A}^{\mathbf{I}}{}_{c} = 0 \quad (2)$$

where subscript *c* represents a magnetic quantity generated by the stator currents. The vector potential ($\mathbf{A}_{pm}$) produced by the PMs only has *z* (axial)-components and is given by

$$\mathbf{A}^{\mathbf{I,II}}{}_{pm} = A^{I,II}{}_{pm}(r)\sin(\theta_r)\mathbf{i}_z \quad (3)$$

By substituting (3) into (1), we can obtain $A^{I,II}{}_{pm}(r)$. The vector potential ($\mathbf{A}_c$) produced by stator currents also only has *z* (axial)-components and is given by

$$\mathbf{A}^{\mathbf{I}}{}_{c} = \sum_{n=1,odd}^{\infty} A^{I}{}_{c}(r)\cos(n\theta_s)\mathbf{i}_z \quad (4)$$

where *n* is the n^{th}-order space harmonic. By substituting (4) into (2), we can also obtain $A^{I}{}_{c}(r)$. In conclusion, by substituting (3) into the definition of the magnetic vector potential, namely, $\nabla \times \mathbf{A} = \mathbf{B}$, the normal ($\mathbf{B}^{r}{}_{pm}$) and tangential ($\mathbf{B}^{\theta}{}_{pm}$) air-gap flux densities produced by the PMs can be obtained as

$$\mathbf{B}^{r}{}_{pm} = \frac{1}{r} A^{I}_{pm}(r)\cos(\theta_r)\mathbf{i}_r;$$
$$\mathbf{B}^{\theta}{}_{pm} = -\frac{\partial}{\partial r} A^{I}_{pm}(r)\sin(\theta_r)\mathbf{i}_\theta \quad (5)$$

In a similar manner, by substituting (4) into $\nabla \times \mathbf{A} = \mathbf{B}$, the normal ($\mathbf{B}^r_c$) and tangential ($\mathbf{B}^\theta_c$) air-gap flux densities produced by the stator currents can be also obtained as

$$\mathbf{B}^r_c = -\sum_{n=1,odd}^{\infty} \frac{n}{r} A^I_c(r)\sin(n\theta_s)\mathbf{i_r};$$
$$\mathbf{B}^\theta_c = -\sum_{n=1,odd}^{\infty} \frac{\partial}{\partial r} A^I_c(r)\cos(n\theta_s)\mathbf{i_\theta} \quad (6)$$

Since the current density **J** is not included in (2) because of the current sheet assumption, this source term should be included in the boundary condition as $\mathbf{B}^\theta_c(R_s, \theta_s) = -\mu_0 J$. Using (5), (6) and proper boundary conditions, the complete magnetic field solutions produced by PMs and stator winding currents can be derived. The derivation procedures for the magnetic field solutions are omitted in this paper because those have already been described in more detail by many researchers [5-7].

3.2 Back-emf and Synchronous Inductance

The flux (λ_{pm}) linking the stator coil of one phase winding owing to the PMs is calculated from [8]

$$\lambda_{pm}(t) = \Lambda_0 N_s l_a \int_{-\alpha_y/2}^{\alpha_y/2} \mathbf{B}^r_{pm}(R_s, \theta_r) r d\theta_s$$
$$= \Lambda_0 N_s R_s l_a \int_{-\alpha_y/2}^{\alpha_y/2} \mathbf{B}^r_{pm}(R_s, \theta_s, t) d\theta_s \quad (7)$$

where Λ_0 is the average value of relative permeance used to account for the reduction of the effective flux density and is given fully in Ref. 9. N_s is the number of turns per coil of a given phase, and α_y is the coil pitch angle. The total flux (Ψ_{pm}) linking all coils per phase is given by $N_c K_{dn} \lambda_{pm}$. Here N_c and K_{dn} are the number of coils of one phase winding and the coil distribution factor, respectively. Therefore, the induced back-emf (e_{back}) per phase is obtained from (7) by $e_{back} = -d\Psi_{pm}/dt = k_e \omega_r$. Here, k_e is the back-emf constant in (V·s/rad).The total flux (Ψ_c) linking all coils per phase owing to the corresponding phase current (i_{ph}) is calculated

$$\Psi_c = N_c K_{dn} \lambda_c = N_c K_{dn} \Lambda_0 N_s l_a R_s \int_{-\alpha_y/2}^{\alpha_y/2} \mathbf{B}^r_{ca}(R_s, \theta_s) d\theta_s \quad (8)$$

It should be noted that $\mathbf{B}^r_{ca}(R_s, \theta_s)$ is the flux density produced by only phase current i_{ph}. The air-gap inductance (L_a) is obtained from (8) by $\Psi_c = L_a i_{ph}$. The self-inductance (L_{self}) is given by the sum of the air-gap inductance (L_a) and the end-winding inductance (L_{end}). If leakage inductance (L_{sl}) is neglected, the synchronous inductance (L_s) is given by $3L_{self}/2$ because mutual inductance (M) is given by $-L_{self}/2$ for synchronous machines. Descriptions for the inductances referred to above are fully presented in Ref. 10.

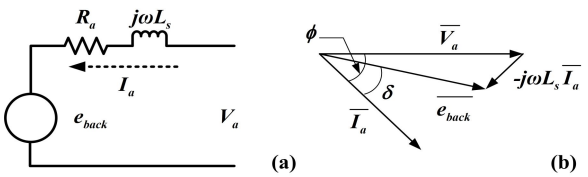

Fig. 3. (a) Equivalent circuit for one phase of HSPM motor and (b) its phasor diagram

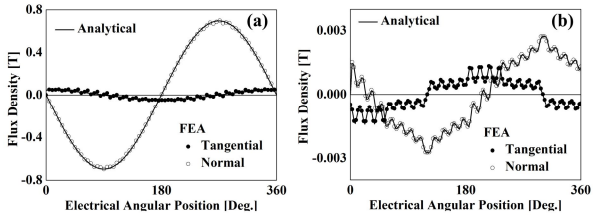

Fig. 4. Comparisons of analytical predictions with FE calculations for normal and tangential flux density at $r = R_e$ produced by (a) the PMs and (b) stator currents

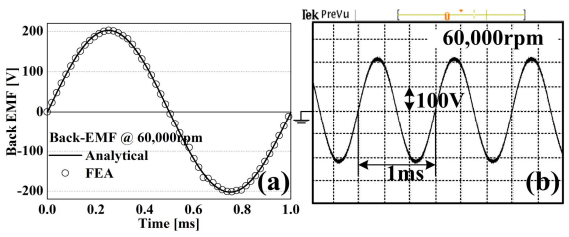

Fig. 5. Back-emf at 60,000 rpm: (a) comparison of predictions with FE calculations and (b) measurements

3.3 Electromagnetic Torque

The electromagnetic torque (T_e) of a PM synchronous motor (PMSM) is given by [11]

$$T_e = 1.5 k_e i_q = 1.5 k_e i_a \cos(\delta) \quad (9)$$

where i_q and i_a are the q-axis current and the peak value of the phase current, respectively. As can be seen from (9), the value of δ should be zero in order to maximize torque capability. However, in spite of efforts to control δ, it is difficult to fix δ at zero because of position estimation errors due to the sensorless drive. Therefore, the calculation of δ provides important information, both for accurate torque calculation and for accurate position estimation for

the control of δ.

Figure 3 (a) shows the equivalent circuit for one phase of the HSPM motor. Here V_a, R_a, and ω are the terminal voltage, phase resistance, and electrical angular frequency, respectively. The corresponding phasor diagram for this equivalent circuit is shown in Fig. 3(b), where R_a has been neglected because its value in HSPM motor is very small (R_a = 40 mΩ in our model). The symbol ¯ denotes phasors, and ϕ is the power factor angle. The voltage equation is obtained from Fig. 3 as

$$\overline{e_{back}} = \overline{V_a} - j\omega L_s \overline{I_a} \tag{10}$$

(10) can be written in phasor notation as

$$e_{back}\angle -(\phi - \delta) = V_a\angle 0^\circ + \omega L_s I_a \angle -(\phi + 90^\circ) \tag{11}$$

By applying Euler's formula and exponential polar form to (11), the internal angle can be obtained as

$$\delta = \phi - \tan^{-1}\left(\frac{\omega L_s I_a \cos(\phi)}{V_a - \omega L_s I_a \sin(\phi)}\right) \tag{12}$$

By using (12) and measuring phase voltage (V_a), phase current (I_a), and the power factor ($\cos(\phi)$), we can easily obtain the value of the internal angle (δ).

TABLE I. Comparison of predictions with FE calculations and measurements for circuit parameters

Parameters \ Methods			Analytical	FE	Test
Back-emf constant (V·rad/s)			0.032	0.032	0.0318
Synchronous Inductance (uH)	L_{self} (uH)	L_a (uH)	38	36	60
		L_{end} (uH)	2	-	
	M (uH)		19	18	

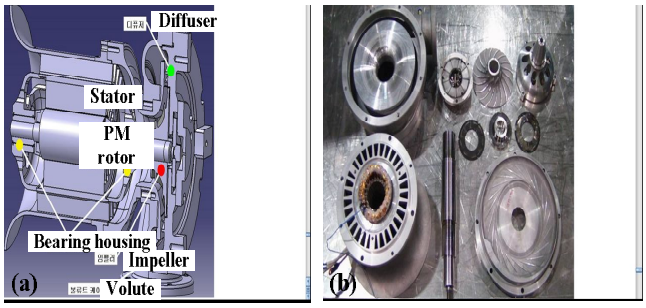

Fig. 6. Air compressor with HSPM motor: (a) aschematic (b) an actual manufactured components

TABLE II. Measured electrical input data of HSPM motor obtained under compressor load conditions

Rotor speed (rpm)	Phase voltage (V)	Phase current (A)	Power (W)
40,000	105.1	11.30	2,620
44,000	114.4	11.86	2,900
46,000	118.4	12.50	3,270
50,000	126.5	13.58	4,090
54,000	134.0	14.62	5,010
58,000	141.5	16.16	6,050
60,000	145.0	16.22	6,320

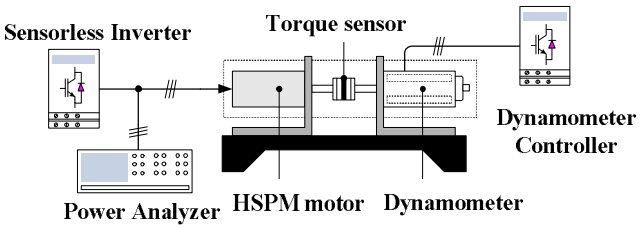

Fig. 7. Schematic of an experimental setup to confirm the validity of torque calculations

4. Results and Discussion

4.1 Circuit Parameters

Figures 4(a) and (b) show comparisons of the analytical predictions with FE calculations for the flux density at $r = R_e$ produced by the PMs and stator winding currents. The analytical results are shown to be in good agreement with FE results. Therefore, the analytical results for back-emf at 60,000 rpm (as shown in Fig. 5) and the circuit parameters (listed in Table I) have also been validated extensively with FE analyses and measurements. It should be noted in Table I that the end- winding inductance (L_{end}) value is calculated by using a simple formula presented in Ref. 10.

4.2 Electromagnetic Torque

Figure 6 shows the schematic and actual manufactured components of the air compressor system with HSPM motor. Table II lists the measured electrical input data of the HSPM motor under compressor load (illustrated in Fig. 6) for various rotor speeds. It should be noted that the value of voltage and current is expressed as an effective value. As can be seen from Table II, the input power of the HSPM motor is proportional to the square of the rotor speed owing to the characteristics of the compressor load.

Figure 7 shows a schematic of the testing apparatus used to measure the torque and electrical input data. The measurement procedure is as follows: (1) the HSPM motor

is coupled with the dynamometer, which is operated at a uniform speed. (2) The torque of the dynamometer is adjusted by the dynamometer's controller to find the electrical quantities that match the corresponding electrical input data presented in Table II at the rotor speed used in step 1. (3) The torque is read from the amplified output of a torque sensor.

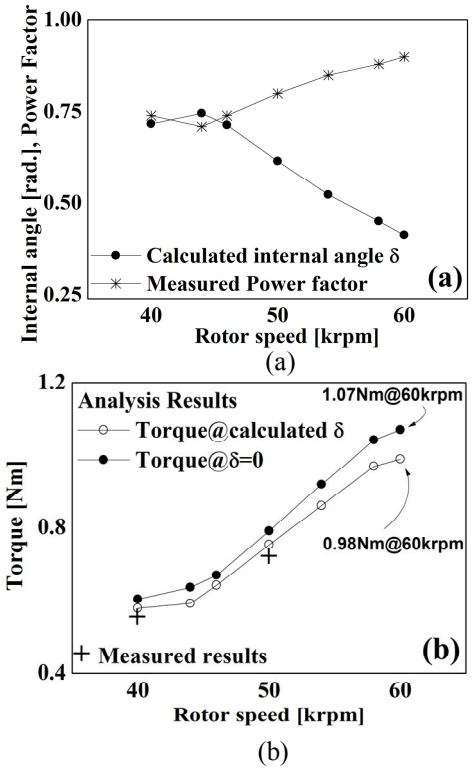

Fig.8. (a) Variation of measured power factor and calculated internal angle and (b) comparison of calculated torque for various values of δ with measured torque versus rotor speed

Figure 8(a) shows the variation in the power factor obtained from Table II and the internal angle (δ) calculated from (12), both as functions of the rotor speed. It can be seen that the value of the internal angle (δ) decreases with an increase in the value of the power factor. This means that as the power factor is increased, the error of position estimation decreases.

Figure 8(b) shows, for various rotor speeds, (1) the torque calculated analytically at δ = 0 (indicated by filled circles), (2) the torque calculated on the basis of the values of δ presented in Fig. 8(a) (indicated by open circles), and (3) the torque measured by using the experimental setup shown in Fig. 7 (indicated by the crosses). The torque analysis results based on estimates of δ are shown to be in better agreement with the measurements. Moreover, when δ = 0, the output torque calculated at 60,000 rpm is 1.07 N·m, resulting in an output power of 6720 W. This output power is higher than the input power (6320W) at 60,000 rpm, as presented in Table II, whereas the output power calculated considering δ at 60,000 rpm is 6154 W. Therefore, it can be concluded that torque analysis methods presented in this paper are very reasonable and, in particular, are useful for the torque prediction of the HSPM motor under compressor load, when it is difficult to measure the torque.

5. Conclusion

An analytical torque calculation of the HSPM motor based on the power factor angle has been described. Based on this analytical approach, the magnetic fields due to the PMs and stator winding currents, back-emf, and synchronous inductance of the HSPM motor have been calculated. In addition, accurate torque calculation of the HSPM motor has been performed by considering the internal angle (δ) calculated from analytical circuit parameters and the measured power factor. Finally, the results from an FE calculation and experimental results obtained from a developed HSPM motor have been presented, confirming the validity of the proposed torque analysis scheme.

Acknowledgements

This research was supported by Basic Science Research Program through the National Research Foundation of Korea (**NRF**) funded by the Ministry of Education, Science and Technology. (*No. 2011-0013398*)

References

[1] K. Ng, Z. Q. Zhu, and D. Howe, "Open-circuit field distribution in a brushless motor with diametrically magnetized PM rotor, accounting for slotting and eddy currents effects." *IEEE Trans. Magn.*, vol. 32, no. 5, pp. 5070-5072, Sept. 1996.

[2] J. Gan, K. T. Chau, Y. Wang, C. C. Chan, and J. Z. Jing, "Design and analysis of a new permanent magnet brushless dc machine," *IEEE Trans. Magn.*, vol. 36, no. 5, pp. 3353-3356, Sept. 2000.

[3] Jiabin Wang, Geraint W. Jewell, and David Howe, "A general framework for the analysis and design of tubular linear permanent magnet machines," *IEEE Trans. Magn*., vol. 35, no. 3, pp.1986-2000, May. 1999.

[4] J. R. Melcher, Continuum Electro-mechanics. Cambridge, MA : MIT Press, 1981.

[5] K. F. Rasmussen, "Analytical Prediction of Magnetic Field from Surface Mounted Permanent Magnet Motors," *In. Proc. Int. Electrical Machines and Drives Conf.*, Seattle, WA, pp.34-36, 1999.

[6] Pierre-Daniel Pfister and Yves Perriard, "Slotless permanent-magnet machines: general analytical magnetic field calculation," *IEEE Trans. Magn.*, vol.47, no.6, pp.1739-1752, June. 2011.

[7] Adel Bellara, Yacine Amara, Georges Barakat, and Brayima Dakyo, "Two-dimensional exact analytical solution of armature reaction field in slotted surface mounted PM radial flux synchronous machines," *IEEE Trans. Magn.*, vol.45, no.10, pp.4534-4538, Oct. 2009.

[8] Z. Q. Zhu, D. Howe, "Instaneous magnetic field distribution in brushless permanent magnet dc motors, Part IV : Magnetic field on load," *IEEE Trans. Magn.*, vol.29, no.1, pp.153-158, Jan. 1993.

[9] Z. Q. Zhu, D. Howe, "Instantaneous magnetic field distribution in brushless permanent magnet dc motors, Part III: Effect of stator slotting," *IEEE Trans. Magn.*, vol.29, no.1, pp.143-151, Jan. 1993.

[10] J.R.Hendershor Jr., and T.J.E.Miller, *Design of brushless permanent-magnet motors*, Oxford, 1994.

[11] R. Krishnan, *Permanent Magnet Synchronous and Brushless DC Motor Drives*, CRC Press, 2010.

Jang-Young Choi received his B.S., M.S., and Ph.D. degrees from Chungnam National University in 2003, 2005, and 2009, respectively. In 2009, he worked as a senior researcher in Halla Climate Control Corporation. He is currently an assistant professor in the department of electrical engineering of Chungnam national university in Korea. His interests are in the design, analysis, simulation, and implementation of linear and rotary motors and preferment magnet generators.

Seok-Myeong Jang received his B.S., M.S., and Ph.D. degrees from Hanyang University in 1976, 1978, and 1986, respectively. Since 1980, he has been with the Department of Electrical Engineering of Chungnam National University in Korea. He is the director of smart electro mechanical Systems (SEMS) Lab. He was a visiting professor in the Department of Electrical Engineering, Kentucky University in 1989. His interests are in the design and analysis of linear machines, high speed machines, smart electro-mechanical systems, and linear oscillating actuators. Dr. Jang is a fellow member of KIEE.

Sung-Ho Lee received his B.S., M.S. and Ph.D. degrees in Electrical Engineering from Chungnam National University in 1997, 1999 and 2003, respectively. During 2003~2007, He worked in the LG D/A Research Lab as a senior researcher. He is currently a lead reseacher in the Gwangju R&D center of Korea Institute of Industrial Technology. His research interests are design and analysis of linear machines and automatic electric machine performance monitoring.